7 Metal, Ceramic, and Carbon Matrix Composites

In the earlier chapters of this book, we considered the performance, manufacturing, and design issues pertaining to polymer matrix composites. In this chapter, we review the thermomechanical properties of metal, ceramic, and carbon matrix composites and a few important manufacturing methods used in producing such composites.

The history of development of metal, ceramic, and carbon matrix composites is much more recent than that of the polymer matrix composites. Initial research on the metal and ceramic matrix composites was based on continuous carbon or boron fibers, but there were difficulties in producing good quality composites due to adverse chemical reaction between these fibers and the matrix. With the development of newer fibers, such as silicon carbide or aluminum oxide, in the early 1980s, there has been a renewed interest and an accelerated research activity in developing the technology of both metal and ceramic matrix composites. The initial impetus for this development has come from the military and aerospace industries, where there is a great need for materials with high strength-to-weight ratios or high modulus-to-weight ratios that can also withstand severe high temperature or corrosive environments. Presently, these materials are very expensive and their use is limited to applications that can use their special characteristics, such as high temperature resistance or high wear resistance. With developments of lower cost fibers and more cost-effective manufacturing techniques, it is conceivable that both metal and ceramic matrix composites will find commercial applications in automobiles, electronic packages, sporting goods, and others.

The carbon matrix composites are more commonly known as carbon–carbon composites, since they use carbon fibers as the reinforcement for carbon matrix. The resulting composite has a lower density, higher modulus and strength, lower coefficient of thermal expansion, and higher thermal shock resistance than conventional graphite. The carbon matrix composites have been used as thermal protection materials in the nose cap and the leading edges of the wing of space shuttles. They are also used in rocket nozzles, exit cones, and aircraft brakes, and their potential applications include pistons in

internal combustion engines, gas turbine components, heat exchangers, and biomedical implants.

7.1 METAL MATRIX COMPOSITES

The metal matrix composites (MMC) can be divided into four general categories:

1. Fiber-reinforced MMC containing either continuous or discontinuous fiber reinforcements; the latter are in the form of whiskers with approximately 0.1–0.5 μm in diameter and have a length-to-diameter ratio up to 200.
2. Particulate-reinforced MMC containing either particles or platelets that range in size from 0.5 to 100 μm. The particulates can be incorporated into the metal matrix to higher volume fractions than the whiskers.
3. Dispersion-strengthened MMC containing particles that are <0.1 μm in diameter.
4. In situ MMC, such as directionally solidified eutectic alloys.

In this chapter, we focus our attention on the first two categories, more specifically on whisker- and particulate-reinforced MMCs. More detailed informations on MMC can be found in Refs. [1–4].

Continuous carbon or boron fiber-reinforced MMCs have been under development for >20 years; however, they have found limited use due to problems in controlling the chemical reaction between the fibers and the molten metal at the high processing temperatures used for such composites. The result of this chemical reaction is a brittle interphase that reduces the mechanical properties of the composite. Fiber surface treatments developed to reduce this problem increase the cost of the fiber. Additionally, the manufacturing cost of continuous carbon or boron fiber-reinforced MMC is also high, which makes them less attractive for many applications. Much of the recent work on MMC is based on silicon carbide whiskers (SiC_w) or silicon carbide particulates (SiC_p). SiC is less prone to oxidative reactions at the processing temperatures used. Furthermore, not only they are less expensive than carbon or boron fibers, but also they can be incorporated into metal matrices using common manufacturing techniques, such as powder metallurgy and casting.

7.1.1 Mechanical Properties

In Chapter 2, we discussed simple micromechanical models in relation to polymer matrix composites in which fibers carry the major portion of the composite load by virtue of their high modulus compared with the polymer matrix, such as epoxy. The same micromechanical models can be applied to MMC with some modifications. The modulus of metals is an order of magnitude higher than that of polymers (Table 7.1). Many metals are capable of

TABLE 7.1
Properties of Some Metal Alloys Used in Metal Matrix Composites

Material	Density, g/cm^3	Tensile Modulus, GPa (Gsi)	YS, MPa (ksi)	UTS, MPa (ksi)	Failure Strain, %	CTE 10^{-6} per °C	Melting Point, °C
Aluminum alloy							
2024-T6	2.78	70 (10.1)	468.9 (68)	579.3 (84)	11	23.2	
6061-T6	2.70	70 (10.1)	275.9 (40)	310.3 (45)	17	23.6	
7075-T6	2.80	70 (10.1)	503.5 (73)	572.4 (83)	11	23.6	
8009	2.92	88 (12.7)	407 (59)	448 (64.9)	17	23.5	
380 (As cast)	2.71	70 (10.1)	165.5 (24)	331 (48)	4	—	540
Titanium alloy							
Ti-6A1-4V (Solution-treated and aged)	4.43	110 (16)	1068 (155)	1171 (170)	8	9.5	1650
Magnesium alloy							
AZ91A	1.81	45 (6.5)	158.6 (23)	234.5 (34)	3	26	650
Zinc–aluminum alloy							
ZA-27 (Pressure die-cast)	5	78 (11.3)	370 (53.6)	425 (61.6)	3	26	375

undergoing large plastic deformations and strain hardening after yielding. In general, they exhibit higher strain-to-failure and fracture toughness than polymers. Furthermore, since the processing temperature for MMCs is very high, the difference in thermal contraction between the fibers and the matrix during cooling can lead to relatively high residual stresses. In some cases, the matrix may yield under the influence of these residual stresses, which can affect the stress–strain characteristics as well as the strength of the composite.

7.1.1.1 Continuous-Fiber MMC

Consider an MMC containing unidirectional continuous fibers subjected to a tensile load in the fiber direction. Assume that the matrix yield strain is lower than the fiber failure strain. Initially, both fibers and matrix deform elastically. The longitudinal elastic modulus of the composite is given by the rule of mixtures:

$$E_L = E_f v_f + E_m v_m. \tag{7.1}$$

After the matrix reaches its yield strain, it begins to deform plastically, but the fiber remains elastic. At this point, the stress–strain diagram begins to deviate from its initial slope (Figure 7.1) and exhibits a new longitudinal modulus, which is given by:

$$E_L = E_f v_f + \left(\frac{d\sigma}{d\varepsilon}\right)_m v_m, \tag{7.2}$$

where $\left(\frac{d\sigma}{d\varepsilon}\right)_m$ is slope of the stress–strain curve of the matrix at the composite strain ε_c. The stress–strain diagram of the composite in this region is not elastic. In addition, it may not be linear if the matrix has a nonuniform strain-hardening rate.

For brittle fiber MMCs, such as SiC fiber-reinforced aluminum alloys, the composite strength is limited by fiber fracture, and the MMCs fail as the composite strain becomes equal to the fiber failure strain. For ductile fiber MMCs, such as tungsten fiber-reinforced copper alloys [5] and beryllium fiber-reinforced aluminum alloys [6], the fiber also yields and plastically deforms along with the matrix. In addition, the composite strength is limited by the fiber failure strain, unless the fibers fail by necking. If the fibers exhibit necking before failure and its failure strain is lower than that of the matrix, the strain at the ultimate tensile stress of the composite will be greater than that at the ultimate tensile stress of the fiber alone.

If the composite failure is controlled by the fiber failure strain, the longitudinal composite strength is given by

$$\sigma_{Ltu} = \sigma_{fu} v_f + \sigma'_m (1 - v_f), \tag{7.3}$$

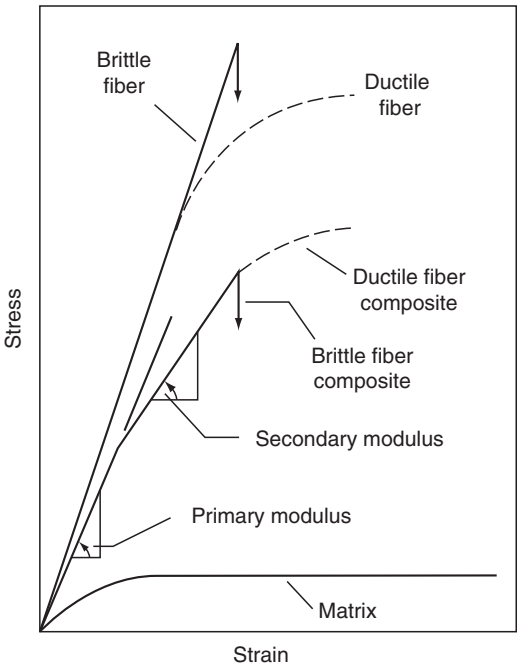

FIGURE 7.1 Schematic representation of longitudinal tensile stress–strain diagram of a unidirectional continuous fiber-reinforced MMC.

where σ'_m is the matrix flow stress at the ultimate fiber strain that is determined from the matrix stress–strain diagram.

Equation 7.3 appears to fit the experimental strength values for a number of MMCs, such as copper matrix composites (Figure 7.2) containing either brittle or ductile tungsten fibers [5]. In general, they are valid for MMCs in which (1) there is no adverse interfacial reaction between the fibers and the matrix that produces a brittle interphase, (2) there is a good bond between the fibers and the matrix, and (3) the thermal residual stresses at or near the interface are low.

The longitudinal tensile strength predicted by Equation 7.3 is higher than the experimental values for carbon fiber-reinforced aluminum alloys. In these systems, unless the carbon fibers are coated with protective surface coating, a brittle Al_4C_3 interphase is formed. Cracks initiated in this interphase cause the fibers to fail at strains that are lower than their ultimate strains. In some cases, the interfacial reaction is so severe that it weakens the fibers, which fail at very low strains compared with the unreacted fibers [7]. If the matrix continues to carry the load, the longitudinal tensile strength of the composite will be

$$\sigma_{Ltu} = \sigma_{mu}(1 - v_f), \tag{7.4}$$

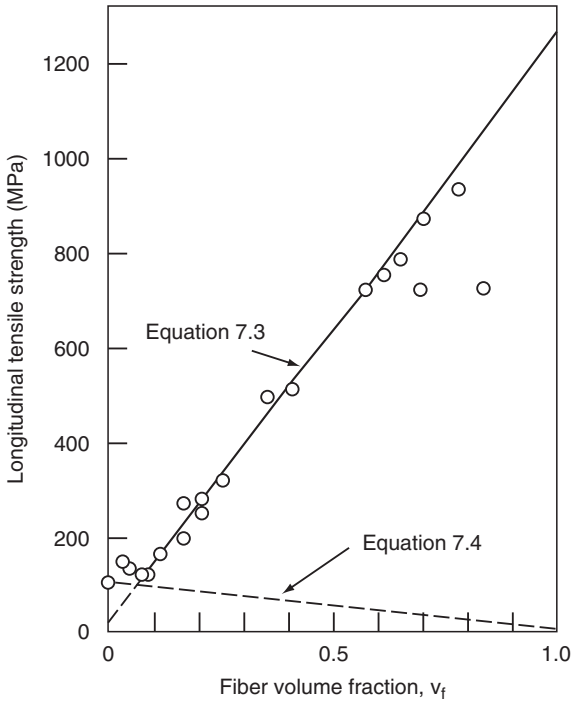

FIGURE 7.2 Longitudinal tensile strength variation of a unidirectional continuous tungsten fiber/copper matrix composite at various fiber volume fractions. (Adapted from Kelly, A. and Davies, G.J., *Metall. Rev.*, 10, 1, 1965.)

which is less than the matrix tensile strength σ_{mu}. Thus, in this case, the matrix is weakened in the presence of fibers instead of getting strengthened (Figure 7.3).

7.1.1.2 Discontinuously Reinforced MMC

In recent years, the majority of the research effort has been on SiC_w- and SiC_p-reinforced aluminum alloys [8]. Titanium, magnesium, and zinc alloys have also been used; however, they are not discussed in this chapter. Reinforcements other than SiC, such as Al_2O_3, have also been investigated. Tensile properties of some of these composites are given in Appendix A.9.

McDanels [9] has reported the mechanical properties of both SiC_w- and SiC_p-reinforced aluminum alloys, such as 6061, 2024/2124, 7075, and 5083. Reinforcement content is in the range of 10–40 vol%. These composites were produced by powder metallurgy, followed by extrusion and hot rolling. His observations are summarized as follows:

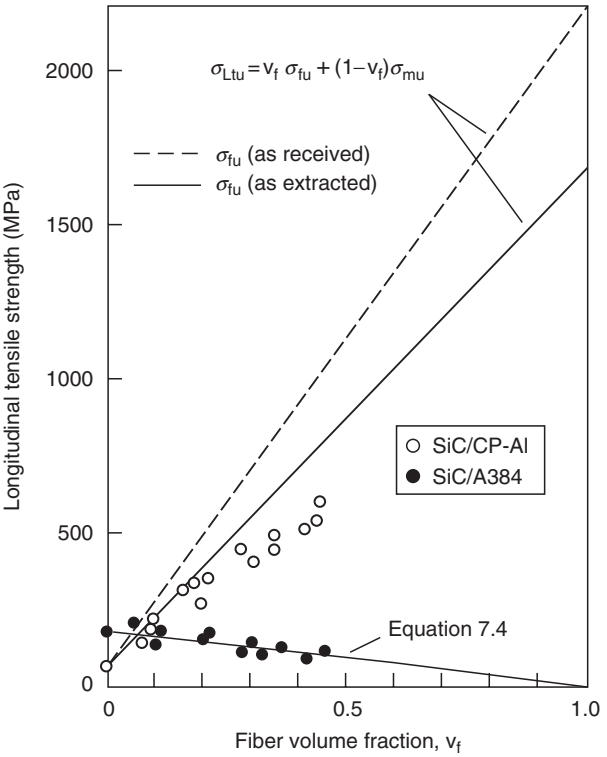

FIGURE 7.3 Longitudinal tensile strength variation of a unidirectional continuous SiC fiber-reinforced high-purity aluminum and A384 aluminum alloy composites at various fiber volume fractions. (Adapted from Everett, R.K. and Arsenault, R.J., eds., *Metal Matrix Composites: Processing and Interfaces*, Academic Press, San Diego, 1991.)

1. The tensile modulus of the composite increases with increasing reinforcement volume fraction; however, the increase is not linear. The modulus values are much lower than the longitudinal modulus predicted by Equation 7.1 for continuous-fiber composites. Furthermore, the reinforcement type has no influence on the modulus.
2. Both yield strength and tensile strength of the composite increase with increasing reinforcement volume fractions; however, the amount of increase depends more on the alloy type than on the reinforcement type. The higher the strength of the matrix alloy, the higher the strength of the composite.
3. The strain-to-failure decreases with increasing reinforcement volume fraction (Figure 7.4). The fracture mode changes from ductile at low volume fractions (below 15%) to brittle (flat and granular) at 30–40 vol%.

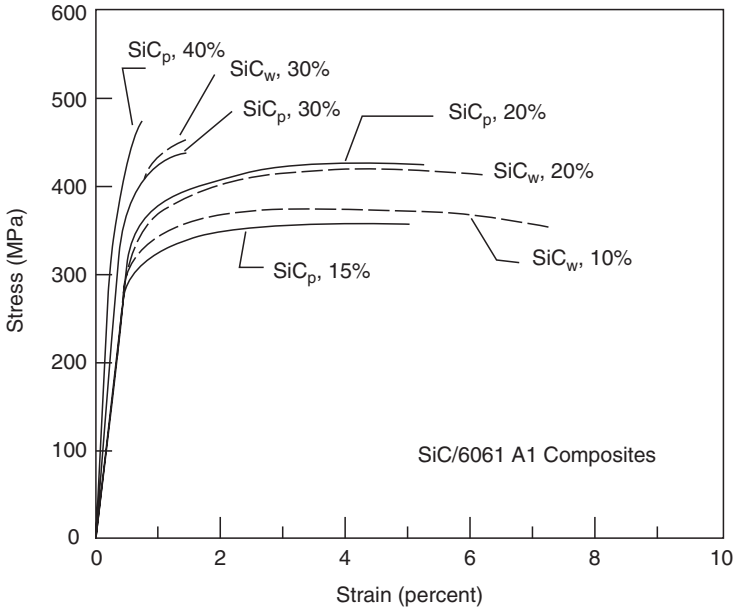

FIGURE 7.4 Tensile stress–strain diagrams of SiC_p- and SiC_w-reinforced 6061-T6 aluminum alloy composites. (Adapted from McDanels, D.L., *Metall. Trans.*, 16A, 1105, 1985.)

McDanels [9] did not observe much directionality in SiC-reinforced aluminum alloys. Since MMCs manufactured by powder metallurgy are transformed into bars and sheets by hot rolling, it is possible to introduce differences in orientation in SiC_w-reinforced alloys with more whiskers oriented in the rolling direction. Repeated rolling through small roll gaps can break whiskers and particulates into smaller sizes, thereby reducing the average particle size or the average length-to-diameter ratio of the whiskers. Both whisker orientation and size reduction may affect the tensile properties of rolled MMCs.

Johnson and Birt [10] found that the tensile modulus of both SiC_p- and SiC_w-reinforced MMCs can be predicted reasonably well using Halpin–Tsai equations (Equations 3.49 through 3.53). However, the strength and ductility of MMCs with discontinuous reinforcements are difficult to model in terms of reinforcement and matrix properties alone, since the matrix microstructure in the composite may be different from the reinforcement-free matrix due to complex interaction between the two. The particle size has a significant influence on yield strength, tensile strength, and ductility of SiC_p-reinforced MMCs [11]. Both yield and tensile strengths increase with decreasing particle size. Such behavior is attributed to the generation of thermal residual stresses, increase in dislocation density, and constraints to dislocation motion, all due to the presence of particles. The ductility of the composite also increases with decreasing

particle size; however, after attaining a maximum value at particle diameters between 2 and 4 μm, it decreases rapidly to low values. The failure of the composite is initiated by cavity formation at the interface or by particle fracture.

Other observations on the thermomechanical properties of SiC_p- or SiC_w-reinforced aluminum alloys are

1. Both CTE and thermal conductivity of aluminum alloys are reduced by the addition of SiC_p [11,12].
2. The fracture toughness of aluminum alloys is reduced by the addition of SiC_p. Investigation by Hunt and his coworkers [13] indicates that fracture toughness is also related to the particle size. They have also observed that overaging, a heat treatment process commonly used for 7000-series aluminum alloys to enhance their fracture toughness, may produce lower fracture toughness in particle-reinforced aluminum alloys.
3. The long-life fatigue strength of SiC_w-reinforced aluminum alloys is higher than that of the unreinforced matrix, whereas that of SiC_p-reinforced aluminum alloys is at least equal to that of the unreinforced matrix (Figure 7.5).
4. The high-temperature yield strength and ultimate tensile strength of SiC-reinforced aluminum alloys are higher than the corresponding values of unreinforced alloys. The composite strength values follow similar functional dependence on temperature as the matrix strength values (Figure 7.6).

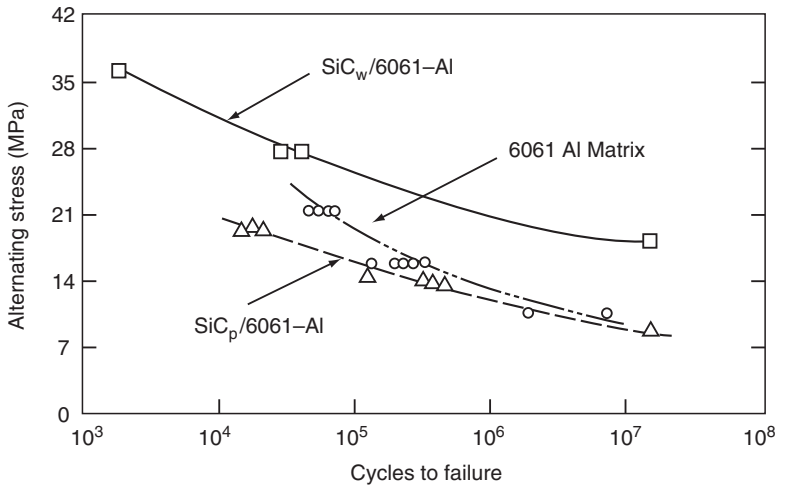

FIGURE 7.5 *S–N* curves for SiC_w- and SiC_p-reinforced 6061 aluminum alloy. (Adapted from Rack, H.J. and Ratnaparkhi, P., *J. Metals*, 40, 55, 1988.)

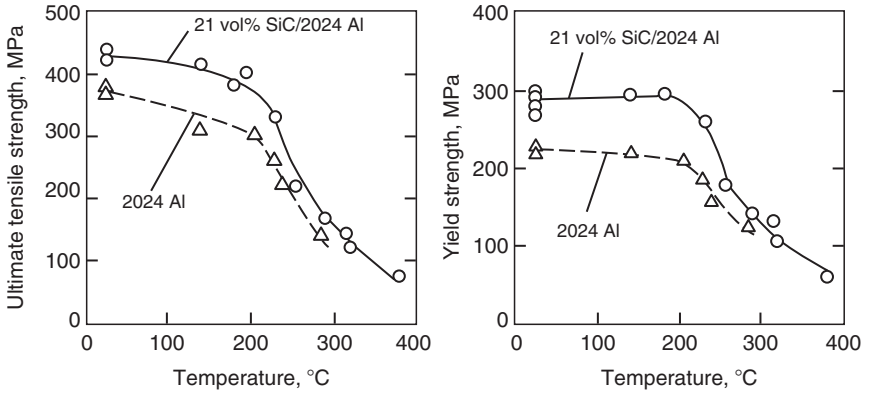

FIGURE 7.6 Effects of increasing temperature on the ultimate tensile strength and yield strength of unreinforced and 21 vol% SiC-reinforced 2024 aluminum alloy. (Adapted from Nair, S.V., Tien, J.K., and Bates, R.C., *Int. Metals Rev.*, 30, 275, 1985.)

5. Karayaka and Sehitoglu [14] conducted strain-controlled fatigue tests on 20 vol% SiC_p-reinforced 2xxx-T4 aluminum alloys at 200°C and 300°C. Based on stress range, the reinforced alloys have a superior fatigue performance than the unreinforced alloys.
6. Creep resistance of aluminum alloys is improved by the addition of either SiC_w or SiC_p. For example, Morimoto et al. [15] have shown that the second-stage creep rate of 15 vol% SiC_w-reinforced 6061 aluminum alloy is nearly two orders of magnitude lower than that of the unreinforced alloy (Figure 7.7).

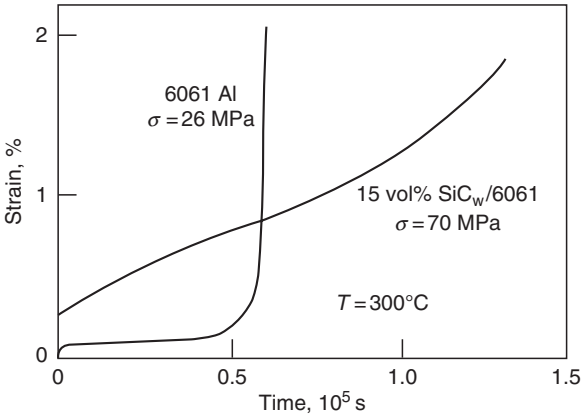

FIGURE 7.7 Comparison of creep strains of unreinforced and 15 vol% SiC_w-reinforced 6061 aluminum alloy. (Adapted from Morimoto, T., Yamaoka, T., Lilholt, H., and Taya, M., *J. Eng. Mater. Technol.*, 110, 70, 1988.)

7.1.2 Manufacturing Processes

7.1.2.1 Continuously Reinforced MMC

Vacuum hot pressing (VHP) is the most common method of manufacturing continuous fiber-reinforced MMC. The starting material (precursor) is made either by drum winding a set of parallel fibers on a thin matrix foil with the fibers held in place by a polymeric binder or by plasma spraying the matrix material onto a layer of parallel fibers that have been previously wound around a drum (Figure 7.8). Sheets are then cut from these preformed tapes by shears or dies and stacked into a layered structure. The fiber orientation in each layer can be controlled as desired.

The layup is inserted into a vacuum bag, which is then placed between the preheated platens of a hydraulic press. After the vacuum level and the temperature inside the vacuum bag reach the preset values, the platen pressure

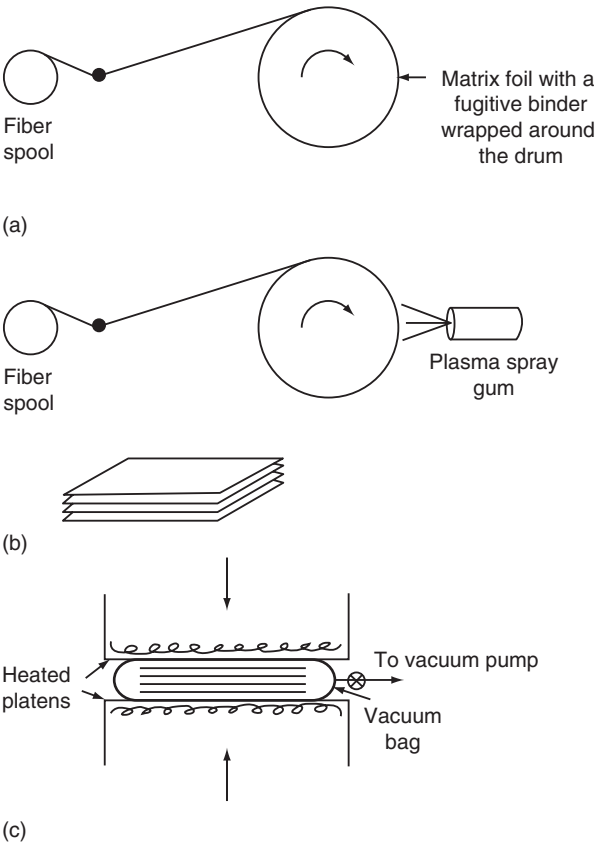

FIGURE 7.8 Schematic of drum winding and vacuum hot pressing for manufacturing continuous-fiber MMC (a) drum winding, (b) cut and stack, and (c) vacuum hot pressing.

is raised and held for a length of time to complete the consolidation of layers into the final thickness. Typically, the temperature is 50%–90% of the solidus temperature of the matrix, and the pressure ranges from 10 to 120 MPa (1.45–17.4 ksi). Afterward, the cooling is carried out at a controlled rate and under pressure to reduce residual stresses as well as to prevent warping.

The consolidation of layers in VHP takes place through diffusion bonding, plastic deformation, and creep of the metal matrix [16]. The basic process parameters that control the quality of consolidation are temperature, pressure, and holding time. Another important parameter is the cleanliness of the layers to be joined. Polymeric binder residues or oxide scales can cause poor bonding between the fibers and the matrix as well as between the matrices in various layers. Therefore, careful surface preparation before stacking the layers can be very beneficial.

7.1.2.2 Discontinuously Reinforced MMC

7.1.2.2.1 Powder Metallurgy

In this process, atomized metal powders (typically with a mean diameter of 15 μm or −325 mesh size) are blended with deagglomerated whiskers or particulates. Deagglomeration may involve agitation of a liquid suspension of the reinforcement in an ultrasonic bath. The blended mixture is cold-compacted in a graphite die, outgassed, and vacuum hot-pressed to form a cylindrical billet. The pressure is applied in the hot-pressing stage only after the temperature is raised above the solidus temperature of the matrix alloy.

Currently available SiC_p-reinforced aluminum billets range from 15 cm (6 in.) to 44.5 cm (17.5 in.) in diameter. Most billets are extruded to rods or rectangular bars using lubricated conical or streamline dies. Various structural shapes can be fabricated from these rods and bars using hot extrusion, while sheets and plates can be produced by hot rolling on conventional rolling mills. Other metalworking processes, such as forging and shear spinning, can also be used for shaping them into many other useable forms.

Typical tensile properties of SiC_w- and SiC_p-reinforced aluminum alloys are given in Table 7.2. All of these composites were manufactured by powder metallurgy and then extruded to rods or bars. Sheets were formed by hot rolling the bars. Following observations can be made from the table:

1. The secondary processing of extrusion and rolling can create significant difference in tensile properties in the longitudinal and transverse directions, especially in whisker-reinforced composites.
2. Ultimate tensile strength, yield strength, and modulus of discontinuously reinforced aluminum alloys increase with increasing reinforcement content, but elongation to failure (which is related to ductility) decreases.
3. For the same reinforcement content, whiskers produce stronger and stiffer composites than particulates.

TABLE 7.2
Tensile Properties of Discontinuously Reinforced Aluminum Alloy Sheets and Extrusions

Material (Alloy/$SiC_{w \text{ or } p}$/vol. frac.-temper)	Orientation	UTS, MPa (ksi)	YS, MPa (ksi)	Elongation, %	Modulus, GPa (Msi)
2009/SiC_w/15%-T8 (Sheet)	L	634 (91.9)	483 (70)	6.4	106 (15.37)
	T	552 (80)	400 (58)	8.4	98 (14.21)
2009/SiC_p/20%-T8 (Sheet)	L	593 (86)	462 (67)	5.2	109 (15.8)
	T	572 (82.9)	421 (61)	5.3	109 (15.8)
6013/SiC_p/15%-T6 (Extrusion)	L	517 (75)	434 (62.9)	6.3	101 (14.64)
6013/SiC_p/20%-T6 (Extrusion)	L	538 (78)	448 (65)	5.6	110 (15.95)
6013/SiC_p/25%-T6 (Extrusion)	L	565 (81.9)	469 (68)	4.3	121 (17.54)
6013/SiC_w/15%-T6 (Extrusion)	L	655 (95)	469 (68)	3.2	119 (17.25)
6090/SiC_p/25%-T6 (Extrusion)	A	483 (70)	393 (57)	5.5	117 (17)
6090/SiC_p/40%-T6 (Extrusion)	A	538 (78)	427 (61.9)	2.0	138 (20)
7475/SiC_p/25%-T6 (Extrusion)	A	655 (95)	593 (86)	2.5	117 (17)

Sources: From Geiger, A.L. and Andrew Walker, J., *J. Metals*, 43, 8, 1991; Harrigan, W.C., Jr., *J. Metals*, 43, 22, 1991.

Notes: L, longitudinal; T, transverse; A, average.

7.1.2.2.2 Casting/Liquid Metal Infiltration

The conventional casting methods can be adopted for producing MMC components for low costs and high production rates. In casting MMC, the liquid metal is poured over a fiber preform and forced to infiltrate the preform either by gravity or by the application of moderate to high pressure. After the infiltration is complete, the liquid metal is allowed to cool slowly in the mold. The pressure is usually applied by means of a hydraulic ram as in die-casting. Vacuum may also be applied to remove air and gaseous by-products of any chemical reaction that may take place between the fibers and matrix as the liquid metal flows into the fiber preform.

Two most important requirements for liquid metal infiltration are (1) the flowing liquid must have a low viscosity and (2) the liquid metal must wet the

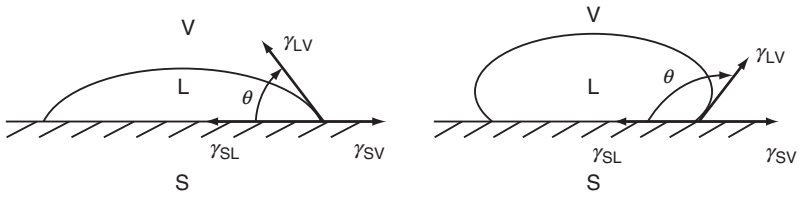

FIGURE 7.9 Surface energy requirement for good fiber surface wetting.

fiber surface. The viscosity of molten aluminum or other alloys is very low (almost two orders of magnitude lower than that of liquid epoxy and five to seven orders of magnitude lower than that of liquid thermoplastics). However, there is, in general, poor wettability between the fibers and the liquid metal, which may affect the infiltration process. The wettability is improved by increasing fiber/atmosphere surface tension or by reducing the liquid metal/fiber surface tension [17]. Both approaches reduce the fiber wetting angle (Figure 7.9) and, therefore, improve wetting between the fibers and the matrix. Common methods of improving wettability are

1. Control the chemical environment in which the infiltration is conducted. For example, controlling the oxygen content of the environment can improve the wettability of aluminum alloys with carbon fibers. This is because aluminum has a strong affinity toward atmospheric oxygen. As the hot liquid metal comes in contact with air, a thin, adherent aluminum oxide layer is formed on its surface, which interferes with wetting.
2. Add an alloying element that modifies or disrupts the surface oxide layer. For example, magnesium added to aluminum alloys disrupts the surface oxide and improves wettability with most reinforcements.
3. Use a coating on the reinforcement surface that promotes wetting. Suitable coatings may also prevent unwanted chemical reaction between the fibers and the matrix. For example, aluminum reacts with carbon fibers above 550°C to form Al_4C_3 platelets, which cause pitting on the carbon fiber surface and reduce the fiber tensile strength.

In general, for high cooling rates and low reinforcement levels (i.e., large interfiber spacings), the matrix microstructure in the solidified MMC is similar to that observed in a reinforcement-free alloy. However, for slower cooling

rates or high reinforcement levels, the matrix microstructure in the MMC can be significantly different from that of the reinforcement-free alloy [18,19]. Some of the observed microstructural differences are

1. Matrix microsegregation may be reduced.
2. The crystal morphology may change from cellular dendritic to completely featureless.
3. Certain primary phases may nucleate preferentially at the reinforcement surface (e.g., silicon in a hypereutectic Al–Si alloy nucleating on the surfaces of carbon fibers or SiC particles).
4. If the reinforcement is relatively mobile, it can be pushed by growing dendrites into the last freezing zone, thereby creating an uneven distribution of the reinforcement in the composite.
5. If the fibers are held below the liquidus temperature of the matrix alloy, the liquid melt is very rapidly cooled as it comes in contact with the fibers and solidification begins at the fiber surface. This leads to finer grain size, which is of the order of the fiber diameter.

7.1.2.2.3 Compocasting

When a liquid metal is vigorously stirred during solidification by slow cooling, it forms a slurry of fine spheroidal solids floating in the liquid. Stirring at high speeds creates a high shear rate, which tends to reduce the viscosity of the slurry even at solid fractions that are as high as 50%–60% by volume. The process of casting such a slurry is called rheocasting. The slurry can also be mixed with particulates, whiskers, or short fibers before casting. This modified form of rheocasting to produce near net-shape MMC parts is called compocasting.

The melt-reinforcement slurry can be cast by gravity casting, die-casting, centrifugal casting, or squeeze casting. The reinforcements have a tendency to either float to the top or segregate near the bottom of the melt due to the differences in their density from that of the melt. Therefore, a careful choice of the casting technique as well as the mold configuration is of great importance in obtaining uniform distribution of reinforcements in a compocast MMC [20].

Compocasting allows a uniform distribution of reinforcement in the matrix as well as a good wet-out between the reinforcement and the matrix. Continuous stirring of the slurry creates an intimate contact between them. Good bonding is achieved by reducing the slurry viscosity as well as increasing the mixing time. The slurry viscosity is reduced by increasing the shear rate as well as increasing the slurry temperature. Increasing mixing time provides longer interaction between the reinforcement and the matrix.

7.1.2.2.4 Squeeze Casting

Squeeze casting is a net-shape metal casting process and involves solidification of liquid metal under pressure. It differs from the more familiar process of

pressure die-casting in which pressure is used only to inject the liquid metal into a die cavity and the solidification takes place under little or no pressure. In squeeze casting, high pressure is maintained throughout solidification. This leads to a fine equiaxed grain structure and very little porosity in the cast component. In general, squeeze-cast metals have higher tensile strengths as well as greater strains-to-failure than the gravity-cast or die-cast metals. In addition, since the use of pressure increases castability, a wide variety of alloy compositions can be squeeze cast, including the wrought alloys that are usually considered unsuitable for casting because of their poor fluidity.

Squeeze casting, as it applies to MMC, starts by placing a preheated fiber preform in an open die cavity, which is mounted in the bottom platen of a hydraulic press. A measured quantity of liquid metal is poured over the preform, the die cavity is closed, and pressure up to 100 MPa is applied to force the liquid metal into the preform. The pressure is released only after the solidification is complete.

Squeeze casting has been used to produce a variety of MMCs, including those with wrought aluminum alloys, such as 2024, 6061, and 7075. However, several investigators [21,22] have suggested that improved properties are obtained by alloy modification of commercial alloys. Other variables that may influence the quality of a squeeze-cast MMC are the temperatures of the molten metal as well as the fiber preform, infiltration speed, and the final squeeze pressure [22,23].

7.2 CERAMIC MATRIX COMPOSITES

Structural ceramics such as silicon carbide (SiC), silicon nitride (Si_3N_4), and aluminum oxide (Al_2O_3) are considered candidate materials for applications in internal combustion engines, gas turbines, electronics, and surgical implants. They are high-modulus materials with high temperature resistance (Table 7.3); however, they have low failure strains and very low fracture toughness. Poor structural reliability resulting from their brittleness and high notch sensitivity is the principal drawback for widespread applications of these materials.

The impetus for developing ceramic matrix composites comes from the possibility of improving the fracture toughness and reducing the notch sensitivity of structural ceramics [24]. Early work on ceramic matrix composites used carbon fibers in reinforcing low- to intermediate-modulus ceramics, such as glass and glass-ceramics. Recent work on ceramic matrix composites has focused on incorporating SiC fibers or whiskers into high-temperature-resistant polycrystalline ceramics, such as SiC and Si_3N_4. Since the modulus values of these materials are close to those of fibers, there is very little reinforcement effect from the fibers. Instead, the heterogeneous nature of the composite contributes to the increase in matrix toughness through several microfailure mechanisms as described in the following section.

TABLE 7.3
Properties of Ceramics and Fibers Used in Ceramic Matrix Composites

Material	Density, g/cm^3	Modulus, GPa (Msi)	Strength, GPa (ksi)	CTE, 10^{-6} per °C	Melting Point, °C
Ceramic matrix					
α-Al_2O_3	3.95	380 (55)	200–310 (29–45)	8.5	2050
SiC	3.17	414 (60)	—	4.8	2300–2500
Si_3N_4	3.19	304 (44)	350–580 (51–84)	2.87	1750–1900
ZrO_2	5.80	138 (20)	—	7.6	2500–2600
Borosilicate glass	2.3	60 (8.7)	100 (14.5)	3.5	—
Lithium aluminosilicate glass-ceramic	2.0	100 (14.5)	100–150 (14.5–21.8)	1.5	—
Fibers					
SiC (Nicalon)	2.55	182–210 (26.4–30.4)	2520–3290 (365.4–477)	—	—
SiC (SCS-6)	3	406 (58.9)	3920 (568.3)	—	—
Al_2O_2 (Nextel-440)	3.05	189 (27.4)	2100 (304.5)	—	—

7.2.1 Micromechanics

Consider a ceramic matrix of modulus E_m containing unidirectional continuous fibers of modulus E_f. Under a tensile load applied in the fiber direction, the initial response of the composite is linear and the composite modulus is given by

$$E_L = E_f v_f + E_m v_m. \tag{7.5}$$

Unlike polymer or metal matrices, the ceramic matrix has a failure strain that is lower than that of the fiber. As a result, failure in ceramic matrix composites initiates by matrix cracking, which originates from preexisting flaws in the matrix. Depending on the fiber strength as well as the fiber–matrix interfacial bond strength, two different failure modes are observed:

1. If the fibers are weak and the interfacial bond is strong, the matrix crack runs through the fibers, resulting in a catastrophic failure of the material. The stress–strain behavior of the composite, in this case, is linear up to failure ((a) in Figure 7.10).
2. If the fibers are strong and the interfacial bond is relatively weak, the matrix crack grows around the fibers and the fiber–matrix interface is debonded (both in front as well as the wake of the matrix crack tip) before the fiber failure. Thus, the matrix crack, in this case, does not result in a catastrophic failure. The ultimate failure of the composite occurs at strains that can be considerably higher than the matrix failure strain.

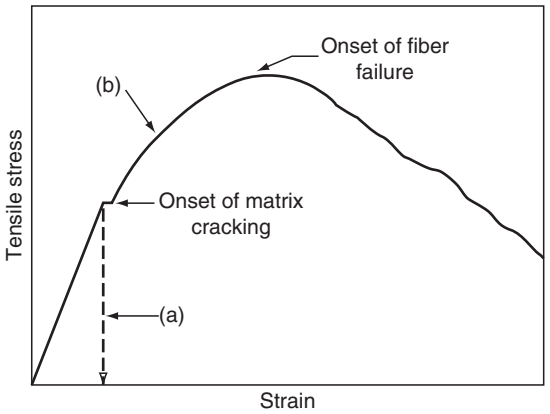

FIGURE 7.10 Schematic tensile stress–strain diagrams of ceramic matrix composites.

Assuming that the failure mode is of the second type, increasing load leads to the formation of multiple matrix cracks [25], which divide the composite into blocks of matrix held together by intact fibers (Figure 7.11). Fibers also form bridges between the crack faces and stretch with the opening of cracks. The stress–strain behavior of the composite becomes nonlinear at the onset of matrix cracking ((b) in Figure 7.10). The ultimate strength of the composite is determined by fiber failure. However, even after the fibers fail, there may be substantial energy absorption as the broken fibers pull out from the matrix. This is evidenced by a long tail in the stress–strain diagram.

The onset of matrix cracking occurs at a critical strain, ε_m^*, which may be different from the matrix failure strain, ε_{mu}. This strain is given by

$$\varepsilon_m^* = \left[\frac{24\gamma_m \tau_i v_f^2 E_f}{d_f(1-v_f)E_m^2 E_L}\right]^{1/3}, \tag{7.6}$$

where

γ_m = fracture energy of the unreinforced matrix
τ_i = fiber–matrix interfacial shear stress (or the resistance to sliding of fibers relative to the matrix)
d_f = fiber diameter
v_f = fiber volume fraction

Once the matrix crack has formed, the stress in the matrix at the crack plane reduces to zero and builds up slowly over a stress transfer length l_m, which is inversely proportional to the fiber–matrix interfacial shear stress. Fiber stress, on the other hand, is maximum at the crack plane and reduces to a lower value

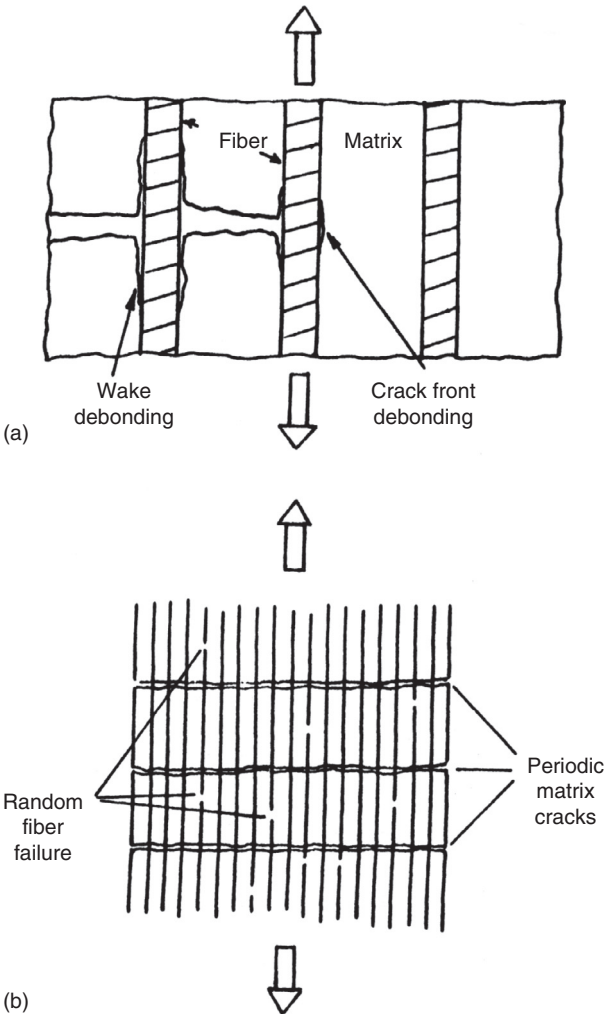

FIGURE 7.11 (a) Debonding and (b) matrix cracking in CMC.

over the same stress transfer length. If the sliding resistance is high, the fiber stress decays rapidly over a small stress transfer length, and the possibility of fiber failure close to the crack plane increases. If the fiber fails close to the crack plane so that the pull-out length is small, the pull-out energy is reduced, and so is the fracture toughness of the composite.

Debonding instead of fiber failure, and subsequently fiber pull-out are essential in achieving high fracture toughness of a ceramic matrix composite.

Evans and Marshall [26] have made the following suggestions for promoting debonding and fiber pull-out:

1. The fracture energy required for debonding, G_{ic}, should be sufficiently small compared with that for fiber fracture, G_{fc}:

$$\frac{G_{ic}}{G_{fc}} \leq \frac{1}{4}.$$

2. Residual radial strain at the interface due to matrix cooling from the processing temperature should be tensile instead of compressive.
3. Sliding resistance between the fibers and the matrix should be small, which means the friction coefficient along the debonded interface should also be small (~0.1).
4. Long pull-out lengths are expected with fibers having a large variability in their strength distribution; however, for high composite strength, the median value of the fiber strength distribution should be high.

As suggested in the preceding discussion and also verified experimentally, the fracture toughness of a ceramic matrix composite is improved if there is poor bonding between the fibers and the matrix. This can be achieved by means of a fiber coating or by segregation at the fiber–matrix interface. The most common method is to use a dual coating in which the inner coating meets the requirements for debonding and sliding, and the outer coating protects the fiber surface from degradation at high processing temperatures.

7.2.2 Mechanical Properties

7.2.2.1 Glass Matrix Composites

Development of ceramic matrix composites began in the early 1970s with carbon fiber-reinforced glass and glass-ceramic composites. Research by Sambell et al. [27,28] on carbon fiber-reinforced borosilicate (Pyrex) glass showed the following results:

1. Increasing fiber volume fraction increases both flexural strength and flexural modulus of the composite containing continuous fibers.
2. The fracture energy of the glass matrix, as measured by the area under the load–deflection diagrams of notched flexural specimens, increases significantly by the addition of continuous carbon fibers. For example, the fracture energy of 40 vol% carbon fiber-borosilicate glass is 3000 J/m^2 compared with only 3 J/m^2 for borosilicate glass. The flexural strength for the same composite is 680 MPa compared with 100 MPa for the matrix alone. The load–deflection diagram for the matrix is linear up

to failure, whereas that for the composite is linear up to 340 MPa. The load–deflection diagram becomes nonlinear at this stress due to matrix cracking on the tension side of the flexural specimen.

3. Random fiber orientation of short carbon fibers produces flexural strengths that are lower than that of borosilicates; however, the fracture energy (work of fracture) increases with fiber volume fraction, as shown in Figure 7.12.

Prewo and Brennan [29] have reported that carbon fiber-reinforced borosilicate glass retains its flexural strength up to 600°C. Above this temperature, the composite strength is reduced due to matrix softening. Thus, although glass matrix is attractive for its lower processing temperature, its application temperature is limited to 600°C. An alternative is to replace glass with a glass-ceramic, such as lithium aluminosilicate (LAS), which increases the use temperature to 1000°C or higher. Since carbon fibers are prone to oxidation above 300°C, they

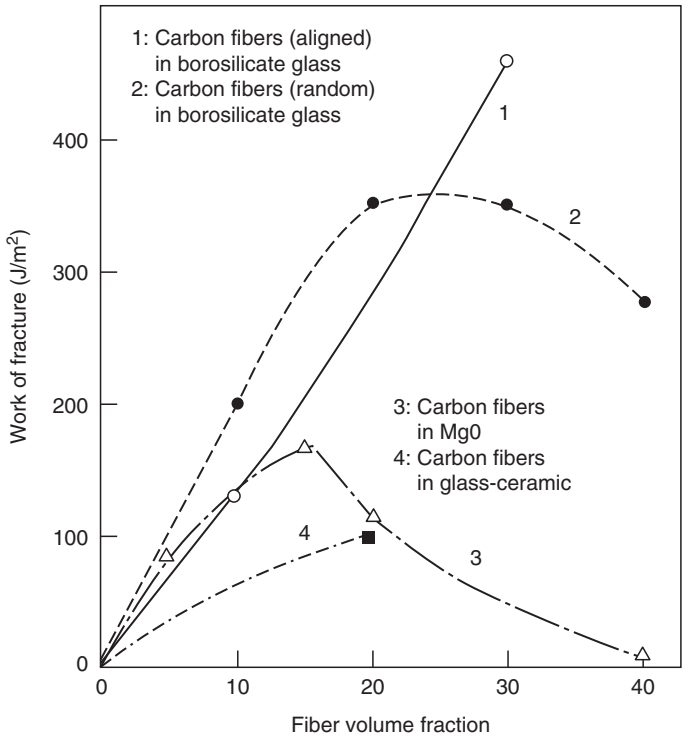

FIGURE 7.12 Work of fracture of various glass matrix composites. (Adapted from Sambell, R.A.J., Bowen, D.H., and Phillips, D.C., *J. Mater. Sci.*, 7, 663, 1972.)

are replaced by SiC fibers, which show no appreciable reduction in either strength or modulus up to 800°C.

Thermomechanical properties of SiC-reinforced glass-ceramics have been studied by a number of investigators [30,31]. The results of investigations on Nicalon (SiC) fiber-reinforced LAS are summarized as follows:

1. Nicalon/LAS composites retain their flexural strength up to 800°C when tested in air, and up to 1100°C when tested in an inert atmosphere, such as argon. The fracture mode of these composites depends strongly on the test environment.
2. Room-temperature tension test in air of unidirectional Nicalon/LAC composites shows multiple matrix cracking and fiber pull-out. The composite fails gradually after the maximum load is reached. When the same composite is tested at 900°C and above, fiber failure occurs after one single matrix crack has formed, resulting in a catastrophic failure with sudden load drop. This change in failure mode is attributed to fiber strength degradation as well as increased fiber–matrix bonding in the oxidative atmosphere. The initial carbon-rich layer between the SiC fiber and the LAS matrix is replaced by an amorphous silicate due to oxidation at 650°C–1000°C. This creates a strong interfacial bond and transforms the composite from a relatively tough material to a brittle material [31].
3. The presence of a carbon-rich interface is very important in obtaining a strong, tough SiC fiber-reinforced LAS composite, since this interface is strong enough to transfer the load from the matrix to the fibers, yet weak enough to debond before fiber failure. This enables the composite to accumulate a significant amount of local damage without failing in a brittle mode.

7.2.2.2 Polycrystalline Ceramic Matrix

Ceramic matrix composites using polycrystalline ceramic matrix, such as SiC, Si_3N_4, and ZrO_2–TiO_2, are also developed. These matrices offer higher temperature capabilities than glasses or glass-ceramics. Research done by Rice and Lewis [32] on unidirectional Nicalon (SiC) fiber-reinforced ZrO_2–TiO_2 and ZrO_2–SiO_2 composites shows the importance of proper fiber–matrix bonding in achieving high flexural strength and fracture toughness in ceramic matrix composites. The BN coating used on Nicalon fibers in their work creates a weaker bond than if the fibers are uncoated. The composite with coated fibers has a flexural strength of 400–900 MPa (60–125 ksi), compared with 70–220 MPa (10–32 ksi) for uncoated fibers. The difference in flexural load–deflection diagrams of coated and uncoated fiber composites is shown in Figure 7.13. The coated fibers not only increased the strength but also created a noncatastrophic failure mode with significant fiber pull-out. Fracture toughness of coated fiber

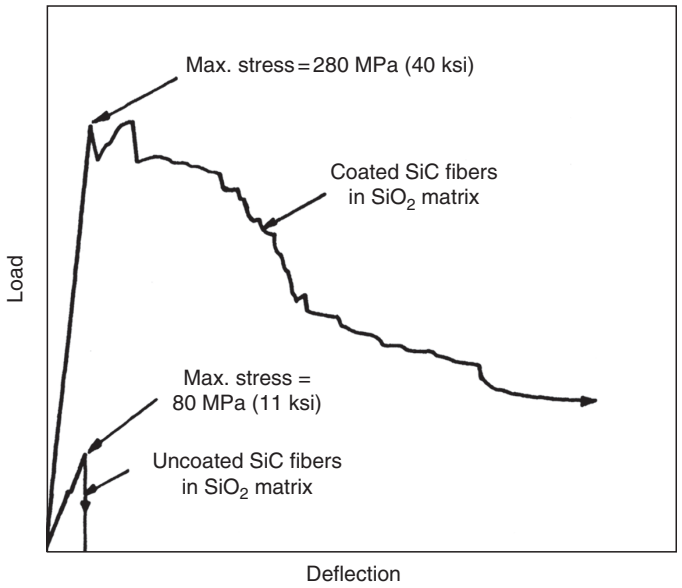

FIGURE 7.13 Effect of fiber surface coating on the room temperature flexural load-deflection diagrams of SiC (Nicalon)-reinforced SiO_2. (Adapted from Rice, R.W. and Lewis, D., III, *Reference Book for Composites Technology*, Vol. 1, S.M. Lee, ed., Technomic Pub. Co., Lancaster, PA, 1989.)

composites is >20 MPa $m^{1/2}$, compared with about 1 MPa $m^{1/2}$ for uncoated fiber composites.

Thomson and LeCostaonec [33] reported the tensile and flexural properties of Si_3N_4 matrix reinforced with unidirectional and bidirectional SiC monofilaments. The fibers are designated as SCS-6 (filament diameter = 140 μm) and SCS-9 (filament diameter = 75 μm), both having a double carbon-rich layer on the outside surface. The purpose of the double layer is to enhance the fiber strength as well as to promote debonding. As demonstrated in Figure 7.14, SCS-reinforced Si_3N_4 composites exhibit considerable load-carrying capability and toughness beyond the initial matrix microcracking at both 23°C and 1350°C.

7.2.3 Manufacturing Processes

The manufacturing processes for ceramic matrix composites can be divided into two groups.

7.2.3.1 Powder Consolidation Process

This is a two-step process of first making a "green" compact, followed by hot pressing the compact into the final shape (Figure 7.15). Hot pressing at

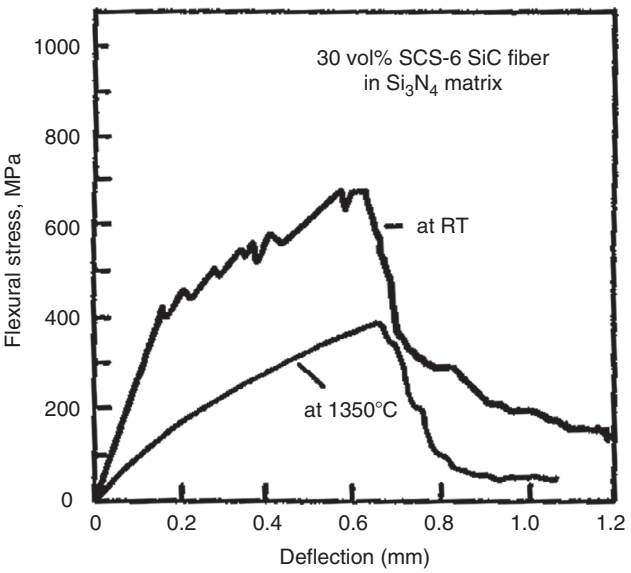

FIGURE 7.14 Flexural stress–deflection diagrams of unidirectional 30 vol% SiC (SCS-6)-reinforced hot-pressed Si_3N_4. (Adapted from Thomson, B. and LeCostaonec, J.F., *SAMPE Q.*, 22, 46, 1991.)

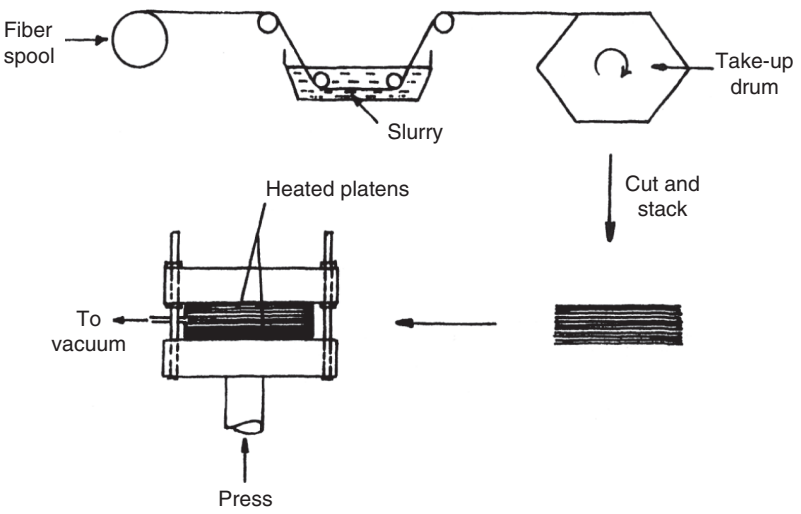

FIGURE 7.15 Powder consolidation process for manufacturing CMC.

temperatures ranging from 1200°C to 1600°C is used to consolidate the compact into a dense material with as little porosity as possible.

There are various ways of making the green compact. For continuous fibers, the compact is made by stacking a number of tapes, which are cut from a sheet of fiber yarns infiltrated with the matrix. The sheet is produced by pulling a row of parallel fiber yarns through a tank containing a colloidal slurry of the matrix and winding it around a drum. The compact can also be made by infiltrating a fiber preform with either a matrix slurry or a colloidal sol prepared from alkoxides and other organic precursors.

The green compact is consolidated and transformed into a dense composite either by VHP in a press or by hot isotactic pressing (HIP) inside an autoclave. VHP is commonly used; however, it is limited to producing only simple shapes, such as plates, rods, or blocks. To reduce porosity in the composite, the hot-pressing temperature is selected in the range of 100°C–200°C higher than that for hot pressing the matrix alone. In some cases, such high temperatures may cause fiber degradation as well as undesirable reactions at the fiber–matrix interface. Rice and Lewis [32] have shown that the strength and toughness of hot-pressed ceramic matrix composites depend strongly on the processing conditions, which include temperature, pressure, and time. Fiber degradation and adverse fiber–matrix reactions can be reduced with a fiber coating as well as by using an inert atmosphere (such as argon) during hot pressing.

The processing temperature is usually lower in HIP. Since pressure is applied equally in all directions instead of uniaxially as in VHP, it is also capable of producing more intricate net-shape structures with higher density and greater uniformity. However, in HIP, the compact must be enclosed in a gas-permeable envelope (called the ''can'') which is removed after processing. Finding a suitable canning material frequently poses a problem.

7.2.3.2 Chemical Processes

Two common chemical processes are chemical vapor infiltration (CVI) and polymer pyrolysis. They are briefly described as follows.

In CVI, the ceramic matrix is deposited on fibers from a gaseous medium by passing it over a preheated fiber preform in a controlled environment. The gas is selected such that it either reacts or decomposes when it comes in contact with the fibers. The temperature range for CVI is 1000°C–1200°C, which is lower than the hot-pressing temperature. For example, SiC matrix can be deposited on SiC fibers by passing methyltrichlorosilane over the SiC fiber preform in the presence of hydrogen at 1200°C [34].

The advantages of CVI are that (1) it can be used to produce a variety of shapes, (2) there is a uniform distribution of matrix in the composite, and (3) fibers undergo less mechanical damage, although the possibility of chemical degradation due to contact with the gas exists. Controlling the porosity in CVI

can be a problem, since pores can seal off between the matrix deposits as they grow from adjacent fibers and impinge on each other.

Polymer pyrolysis is a two-step process of first making a polymer-impregnated preform via standard polymer impregnation techniques, followed by pyrolysis of the polymer at high temperatures to yield the ceramic matrix. For example, the polymer precursor for producing SiC matrix is an organosilicon polymer, such as polycarbosilane or polyborosiloxane.

The pyrolysis temperature is in the range of 700°C–1000°C, which is low compared with that used in hot pressing. Therefore, provided a suitable polymer precursor is available, it is suitable for a wide range of fibers that cannot ordinarily be used with hot pressing. The principal disadvantage is that it results in a highly porous matrix, primarily due to shrinkage cracks originating from the polymerization process during pyrolysis. One method of reducing the polymer shrinkage is to mix it with fine ceramic fillers.

7.3 CARBON MATRIX COMPOSITES

The carbon matrix composites consist of carbon fibers in carbon matrix and are commonly referred to as carbon–carbon (C–C) composites. They are thermally stable up to 3000°C in a nonoxidative environment, but unless protected by a surface coating or chemically modified to provide protection, they oxidize and degrade in presence of oxygen, even at 400°C–500°C. The protection of C–C composites against oxidation at high temperatures requires the use of either an external coating or internal modification. Both oxide coatings, such as SiO_2 and Al_2O_3, and nonoxide coatings, such as SiC, Si_3N_4, and HFB_2, have been used. Low oxygen permeability and thermal expansion matching are the two most critical requirements for the external coating. Thermal expansion mismatch between the coating and the C–C composite may cause cracking in the coating, which in the most severe case may result in spalling of the coating from the C–C composite surface. For applications in oxidizing environments, current coatings limit the maximum use temperature of C–C composites to 1700°C.

Fibers in the C–C composites can be either continuous or discontinuous. Continuous fibers are selected for structural applications. Table 7.4 shows the mechanical and thermal properties of continuous fiber-reinforced C–C composites containing carbon fibers that have strengths up to 2.5 GPa and elastic modulus in the range of 350–450 GPa. For comparison, properties of graphite are also listed in Table 7.4, since graphite is also considered for high temperature applications in which C–C composites are used. As with other fiber-reinforced composites, the tensile and compressive properties of C–C composites depend on the fiber properties and fiber architecture. While they are generally very high, the shear strength and modulus are very low. This is one of the limitations of C–C composites. Another point to note is that the failure strain of the matrix in C–C composites is lower than that of the fibers. Thus if there is a strong bond between the fibers and the matrix in a C–C

TABLE 7.4
Properties of Carbon–Carbon Composites

		Mechanical Properties at 23°C					Thermal Properties	
Material	v_f (%)	Tensile Strength (MPa)	Tensile Modulus (GPa)	Compressive Strength (MPa)	Shear Strength (MPa)	Shear Modulus (GPa)	CTE[a] (10^{-6} per °C)	Thermal Conductivity[b] (W/m°C)
C–C with 1D Unidirectional continuous	65	650–1000 (*x*) 2 (*z*)	240–280 (*x*) 3.4 (*z*)	620 (*x*)	7–14 (*xy*)	4–7 (*xy*)	1.1(*x*) 10.1(*z*)	125 (*x*) 10 (*z*)
C–C with 2D Fabric	31 (*x*) 30 (*y*)	300–350 (*x*) 2.8–5 (*z*)	110–125 (*x*) 4.1 (*z*)	150 (*x*)	7–14 (*xy*)	4–7 (*xy*)	1.3 (*x*) 6.1 (*z*)	95 (*x*) 4 (*z*)
C–C with 3D Woven orthogonal fibers	13 (*x*) 13 (*y*) 21 (*z*)	170 (*x*) 300 (*z*)	55 (*x*) 96 (*z*)	140 (*z*)	21–27 (*xy*)	1.4–2.1 (*xy*)	1.3 (*x*) 1.3 (*z*)	57 (*x*) 80 (*z*)
Graphite		20–30	7.5–11	83			2.8	50

Source: Adapted from Sheehan, J.E., Buesking, K.W., and Sullivan, B.J., *Annu. Rev. Mater. Sci.*, 24, 19, 1994.

[a] Coefficient of thermal expansion between 23°C and 1650°C.
[b] At 800°C.

composite, fibers fail immediately after the matrix fails and the composite fails in a brittle manner with low strength. On the other hand, if the fiber–matrix bond is not very strong, matrix cracking at low strain will not produce immediate fiber failure; instead, there will be energy absorption due to debonding, fiber bridging, fiber fracture, and fiber pull-out, and such a composite can possess high fracture toughness. Indeed, the work of fracture test of fully densified unidirectional C–C composites shows fracture energy value of about 2×10^4 J/m^2 [35]. In comparison, the fracture energy of engineering ceramics and premium-grade graphite is $<10^2$ J/m^2.

Two basic fabrication methods are used for making C–C composites [36]: (1) liquid infiltration and (2) chemical vapor deposition (CVD). The starting material in either of these methods is a carbon fiber preform, which may contain unidirectional fibers, bi- or multidirectional fabrics, or a three-dimensional structure of carbon fibers. In the liquid infiltration process, the preform is infiltrated with a liquid, which on heating, carbonizes to yield at least 50 wt% carbon. In the CVD process, a hydrocarbon gas is infiltrated into the preform at high temperature and pressure. The chemical breakdown of the hydrocarbon gas produces the carbon matrix. In general, CVD is used with thin sections and liquid infiltration is used with thick sections.

Two types of liquids are used in the liquid infiltration method: (1) pitch, which is made from coal tar or petroleum and (2) a thermoset resin, such as a phenolic or an epoxy. In the pitch infiltration method, either an isotropic pitch or a mesophase pitch is infiltrated into the dry carbon fiber preform at 1000°C or higher and at pressure ranging from atmospheric to 207 MPa (30,000 psi). At this temperature, carbonization occurs simultaneously with infiltration. If the carbonization is performed at the atmospheric pressure, the carbon yield is 50–60 wt% with isotropic pitch and >80 wt% with mesophase pitch. The carbon yield is higher if the pressure is increased.

In the thermoset resin infiltration method, the starting material is a prepreg containing carbon fibers in a partially cured thermoset resin. A laminate is first constructed using the prepreg layers and the vacuum bag molding process described in Chapter 5. The resin in the laminate is then carbonized at 800°C–1000°C in an inert atmosphere. The volatiles emitted during the carbonization reaction cause shrinkage and a reduction in density. The carbonization process is performed slowly to prevent rapid evolution of volatiles, which may cause high porosity and delamination between the layers. The infiltration/carbonization process is repeated several times to reduce the porosity and increase the density of the composite. The carbon yield in this process is between 50% and 70% depending on the resin and processing conditions used.

The CVD process starts with the fabrication of a dry fiber preform in the shape of the desired part. The preform is heated in a furnace under pressure (typically around 1 psi or 7 kPa) and in the presence of a hydrocarbon gas, such as methane, propane, or benzene. As the gas is thermally decomposed, a layer of pyrolitic carbon is slowly formed and deposited on the hot preform

surface. In the isothermal CVD process, the temperature of the furnace is maintained constant at 1100°C. Since the pyrolitic carbon deposited on the surface tends to close the pores located at and very close to the surface, it becomes difficult to fill the internal pores with carbon. Thus it may be necessary to lightly machine the preform surfaces to remove the surface carbon layer and then repeat the infiltration process. The infiltration is better if either a thermal gradient or a pressure gradient is created across the thickness of the preform. In the thermal gradient technique, one surface is maintained at a higher temperature than the other, and the carbon infiltration progresses from the hotter surface to the colder surface. In the pressure gradient technique, a pressure differential is created across the thickness, which forces the hydrocarbon gas to flow through the pores in the preform and deposit carbon throughout the thickness. With both these techniques, very little, if any, crust is formed on the surfaces.

The C–C composite obtained by either liquid infiltration or by CVD can be heated further to transform the carbon matrix from amorphous form to graphitic form. The graphitization temperature is between 2100°C and 3000°C. Graphitization increases both strength and modulus of the C–C composite, while the fracture toughness depends on the graphitization temperature. For example, for a pitch-based matrix, the optimum graphitization temperature is 2700°C, above which fracture toughness starts to decrease [37].

Depending on the starting material and the process condition, the microstructure of carbon matrix in C–C composites may vary from small, randomly oriented crystallites of turbostratic carbon to large, highly oriented, and graphitized crystallites. The carbon matrix may also contain large amount of porosity, which causes the density to be lower than the maximum achievable density of approximately 1.8–2 g/cm^3. There may also be microcracks originating from thermal stresses as the C–C composite cools down from the processing temperature to room temperature. Since porosity affects not only the density, but also the properties of the composite, repeated impregnation and carbonization cycles are used to reduce the porosity. This process is often referred to as densification.

REFERENCES

1. R.K. Everett and R.J. Arsenault (eds.), *Metal Matrix Composites: Mechanisms and Properties*, Academic Press, San Diego (1991).
2. R.K. Everett and R.J. Arsenault (eds.), *Metal Matrix Composites: Processing and Interfaces*, Academic Press, San Diego (1991).
3. T.W. Clyne and P.J. Withers, *An Introduction to Metal Matrix Composites*, Cambridge University Press, Cambridge, UK (1993).
4. N. Chawla and K.K. Chawla, *Metal Matrix Composites*, Springer, New York (2006).
5. A. Kelly and G.J. Davies, The principles of the fibre reinforcement of metals, *Metall. Rev., 10*:1 (1965).

6. A. Toy, Mechanical properties of beryllium filament-reinforced aluminum composites, *J. Mater., 3*:43 (1968).
7. M. Taya and R.J. Arsenault, *Metal Matrix Composites: Thermomechanical Behavior*, Pergamon Press, Oxford (1989).
8. S.V. Nair, J.K. Tien, and R.C. Bates, SiC-reinforced aluminum metal matrix composites, *Int. Metals Rev., 30*:275 (1985).
9. D.L. McDanels, Analysis of stress–strain, fracture, and ductility behavior of aluminum matrix composites containing discontinuous silicon carbide reinforcement, *Metall. Trans., 16A*:1105 (1985).
10. W.S. Johnson and M.J. Birt, Comparison of some micromechanics models for discontinuously reinforced metal matrix composites, *J. Compos. Technol. Res., 13*:168 (1991).
11. A.L. Geiger and J. Andrew Walker, The processing and properties of discontinuously reinforced aluminum composites, *J. Metals, 43*:8 (1991).
12. K. Schmidt, C. Zweben, and R. Arsenault, Mechanical and thermal properties of silicon-carbide particle-reinforced aluminum, *Thermal and Mechanical Behavior of Metal Matrix and Ceramic Matrix Composites, ASTM STP, 1080*:155 (1990).
13. J.J. Lewandowski, C. Liu, and W.H. Hunt, Jr., Microstructural effects on the fracture mechanisms in 7xxx A1 P/M-SiC particulate metal matrix composites, *Processing and Properties for Powder Metallurgy Composites* (P. Kumar, K. Vedula, and A. Ritter, eds.), TMS, Warrendale, PA (1988).
14. M. Karayaka and H. Sehitoglu, Thermomechanical fatigue of particulate-reinforced aluminum 2xxx-T4, *Metall. Trans. A, 22A*:697 (1991).
15. T. Morimoto, T. Yamaoka, H. Lilholt, and M. Taya, Second stage creep of whisker/6061 aluminum composites at 573K, *J. Eng. Mater. Technol., 110*:70 (1988).
16. R.K. Everett, Diffusion bonding, *Metal Matrix Composites: Processing and Interfaces*, Chapter 2 (R.K. Everett and R.J. Arsenault, eds.), Academic Press, San Diego (1991).
17. A. Mortensen, J.A. Cornie, and M.C. Flemings, Solidification processing of metal-matrix composites, *J. Metals, 40*:12 (1988).
18. A. Mortensen, M.N. Gungor, J.A. Cornie, and M.C. Flemings, Alloy microstructures in cast metal matrix composites, *J. Metals, 38*:30 (1986).
19. P. Rohatgi and R. Asthana, The solidification of metal-matrix particulate composites, *J. Metals, 43*:35 (1991).
20. P. Rohatgi, Cast aluminum-matrix composites for automotive applications, *J. Metals, 43*:10 (1991).
21. C.R. Cook, D.I. Yun, and W.H. Hunt, Jr., System optimization for squeeze cast composites, *Cast Reinforced Metal Composites* (S.G. Fishman and A.K. Dhingra, eds.), ASM International, Metals Park, OH (1988).
22. T. Kobayashi, M. Yosino, H. Iwanari, M. Niinomi, and K. Yamamoto, Mechanical properties of SiC whisker reinforced aluminum alloys fabricated by pressure casting method, *Cast Reinforced Metal Composites* (S.G. Fishman and A.K. Dhingra, eds.), ASM International, Metals Park, OH (1988).
23. H. Fukunaga, Squeeze casting processes for fiber reinforced metals and their mechanical properties, *Cast Reinforced Metal Composites* (S.G. Fishaman and A.K. Dingra, eds.), ASM International, Metal Park, OH (1988).
24. K.K. Chawla, *Ceramic Matrix Composites*, Chapman & Hall, London (1993).

25. J. Aveston, G.A. Cooper, and A. Kelly, Single and multiple fracture, *The Properties of Fiber/Composites,* IPC Science and Technology Press, Surrey, England (1971).
26. A.G. Evans and D.B. Marshall, The mechanical behavior of ceramic matrix composites, *Acta Metall., 37*:2567 (1989).
27. R.A.J. Sambell, D.H. Bowen, and D.C. Phillips, Carbon fibre composites with ceramic and glass matrices, Part 1: Discontinuous fibres, *J. Mater. Sci., 7*:663 (1972).
28. R.A.J. Sambell, A. Briggs, D.C. Phillips, and D.H. Bowen, Carbon fibre composites with ceramic and glass matrices, Part 2: Continuous fibres, *J. Mater. Sci., 7*:676 (1972).
29. K.M. Prewo and J.J. Brennan, Fiber reinforced glasses and glass ceramics for high performance applications, *Reference Book for Composites Technology*, Vol. 1 (S.M. Lee, ed.), Technomic Pub. Co., Lancaster, PA (1989).
30. J.J. Brennan and K.M. Prewo, Silicon carbide fibre reinforced glass-ceramic matrix composites exhibiting high strength and toughness, *J. Mater. Sci., 17*:2371 (1982).
31. T. Mah, M.G. Mendiratta, A.P. Katz, and K.S. Mazdiyasni, Recent developments in fiber-reinforced high temperature ceramic composites, *Ceramic Bull., 66*:304 (1987).
32. R.W. Rice and D. Lewis III, Ceramic fiber composites based upon refractory polycrystalline ceramic matrices, *Reference Book for Composites Technology*, Vol. 1 (S.M. Lee, ed.), Technomic Pub. Co., Lancaster, PA (1989).
33. B. Thomson and J.F. LeCostaonec, Recent developments in SiC monofilament reinforced Si_3N_4 composites, *SAMPE Q., 22*:46 (1991).
34. R.L. Lehman, Ceramic matrix fiber composites, *Structural Ceramics* (J.B. Wachtman, Jr., ed.), Academic Press, San Diego (1989).
35. J.E. Sheehan, K.W. Buesking, and B.J. Sullivan, Carbon–carbon composites, *Annu. Rev. Mater. Sci*., *24*:19 (1994).
36. J.D. Buckley and D.D. Edie, *Carbon–Carbon Materials and Composites*, William Andrews Publishing, Norwich, NY (1993).
37. D.L. Chung, *Carbon Fiber Composites*, Butterworth-Heinemann, Newton, MA (1994).

PROBLEMS

P7.1. Experimentally determined elastic properties of a unidirectional continuous P-100 carbon fiber-reinforced 6061-T6 aluminum alloy are $E_{11} = 403$ GPa, $E_{22} = 24$ GPa, $\nu_{12} = 0.291$, and $G_{12} = 18.4$ GPa. Fiber volume fraction in the composite is 0.5.

1. Compare these values with theoretical predictions and explain the differences, if any.
2. Using the experimental values, determine the off-axis elastic modulus, E_{xx}, at $\theta = 15°$ and 45° and compare them with the experimental values of 192 and 41 GPa, respectively.

P7.2. Suppose both fibers and matrix in a unidirectional continuous fiber MMC are ductile, and their tensile stress–strain equations are given by the general form:

$$\sigma = K\,\varepsilon^m,$$

where K and m are material constants obtained from experimentally determined stress–strain data. K and m for the fibers are different from K and m for the matrix.

Assuming that the longitudinal stress–strain relationship for the composite can also be described by a similar equation, derive the material constants K and m of the composite in terms of fiber and matrix parameters.

P7.3. Referring to Problem P7.2, determine the stress–strain equation for a unidirectional beryllium fiber-reinforced aluminum alloy. Assume that the fiber volume fraction is 0.4. Material constants for the fiber and the matrix are given as follows:

	K (MPa)	m
Beryllium fiber	830	0.027
Aluminum matrix	250	0.127

P7.4. Referring to Appendix A.2, determine the thermal residual stresses in a unidirectional SCS-6-reinforced titanium alloy ($v_f = 40\%$) and comment on their effects on the failure mode expected in this composite under longitudinal tensile loading. The fabrication temperature is 940°C. Use the following fiber and matrix characteristics in your calculations:

Fiber: $E_f = 430$ GPa, $v_f = 0.25$, $\alpha_f = 4.3 \times 10^{-6}$ per°C,
$\sigma_{fu} = 3100$ MPa, $r_f = 102$ μm.
Matrix: $E_m = 110$ GPa, $v_m = 0.34$, $\alpha_m = 9.5 \times 10^{-6}$ per°C,
$\sigma_{my} = 800$ MPa, $\sigma_{mu} = 850$ MPa, $\varepsilon_{mu} = 15\%$.

P7.5. Using Halpin–Tsai equations, determine the tensile modulus of 20 vol% SiC whisker-reinforced 2024-T6 aluminum alloy for (a) $l_f/d_f = 1$ and (b) $l_f/d_f = 10$. Assume a random orientation for the whiskers.

P7.6. SiC_w-reinforced 6061-T6 aluminum alloy ($v_f = 0.25$) is formed by powder metallurgy and then extruded into a sheet. Microscopic examination of the cross section shows about 90% of the whiskers are aligned in the extrusion direction. Assuming $l_f/d_f = 10$, estimate the tensile modulus and strength of the composite. Make reasonable assumptions for your calculations.

P7.7. Coefficient of thermal expansion of spherical particle-reinforced composites is estimated using the Turner equation:

$$\alpha_c = \frac{v_r K_r \alpha_r + v_m K_m \alpha_m}{v_r K_r + v_m K_m},$$

where

K = Bulk modulus $= \dfrac{E}{3(1-2\nu)}$

v = volume fraction

α = CTE

E = modulus

ν = Poisson's ratio

Subscripts r and m represent reinforcement and matrix, respectively

Using the Turner equation and assuming SiC particulates to be spherical, plot the coefficient of thermal expansion of SiC_P-reinforced 6061 aluminum alloy as a function of reinforcement volume fraction. Assume $\alpha_r = 3.8 \times 10^{-6}$ per °C, $E_r = 450$ GPa, $\nu_r = 0.17$.

For comparison, experimental values of α_c are reported as 16.25×10^{-6} and 10.3×10^{-6} per °C at $v_r = 25\%$ and 50%, respectively.

P7.8. The steady-state (secondary) creep rate of both unreinforced and reinforced metallic alloys has been modeled by the following power-law equation:

$$\dot{\varepsilon} = A\sigma^n \exp\left(-\frac{E}{RT}\right),$$

where

$\dot{\varepsilon}$ = steady-state creep rate (per s)

A = constant

σ = stress (MPa)

n = stress exponent

E = activation energy

R = universal gas constant

T = temperature (°K)

1. Plot the following constant temperature creep data (Ref. [15]) obtained at 300°C on an appropriate graph and determine the values of A and n. Assume the activation energies for 6061 aluminum alloy and SiC_w/6061 as 140 and 77 kJ/mol, respectively.
2. Compare the creep rates of the above two materials at 70 MPa and 250°C.

Material	Stress (MPa)	$\dot{\varepsilon}$ (per s)
6061	26	9.96×10^{-10}
	34	3.68×10^{-9}
	38	6.34×10^{-9}
SiC_w/6061	70	7.36×10^{-9}
($v_f = 15\%$)	86	3.60×10^{-7}
	90	6.40×10^{-7}
	95	2.04×10^{-6}
	100	6.40×10^{-6}

P7.9. A unidirectional Nicalon fiber-reinforced LAS glass matrix composite ($v_f = 0.45$) is tested in tension parallel to the fiber direction. The first microcrack in the matrix is observed at 0.3% strain. Following fiber and matrix parameters are given:
$d_f = 15\ \mu m$, $E_f = 190$ GPa, $\sigma_{fu} = 2.6$ GPa, $E_m = 100$ GPa, $\sigma_{mu} = 125$ MPa, and $\gamma_m = 4 \times 10^{-5}$ MPa m.

Determine (a) the sliding resistance between the fibers and matrix, (b) the stress transfer length, and (c) expected range of spacing between matrix cracks.

P7.10. A continuous fiber-reinforced ceramic matrix composite is tested in three-point flexure. Describe the failure modes you may expect as the load is increased. What material parameters you will recommend to obtain a strong as well as tough ceramic matrix composite in a flexural application.

P7.11. The longitudinal tensile modulus of a unidirectional continuous carbon fiber-reinforced carbon matrix composite is reported as 310 GPa. It is made by liquid infiltration process using epoxy resin. The carbon fiber content is 50% by volume. The carbon fiber modulus is 400 GPa.

1. Calculate the modulus of the carbon matrix and the percentage of the tensile load shared by the carbon matrix. Comment on how this is different from a carbon fiber-reinforced epoxy matrix composite.
2. Assume that the failure strains of the carbon fibers and the carbon matrix are 0.8% and 0.3%, respectively. Estimate the longitudinal tensile strength of the C–C composite. Comment on how this is different from a carbon fiber-reinforced epoxy matrix composite.
3. Using the rule of mixtures, calculate the longitudinal thermal conductivity of the C–C composite. Assume that the thermal conductivity of the carbon fibers is 100 W/m°K and the thermal conductivity of the carbon matrix is 50 W/m°K.